RSC Advances

PAPER

View Article Online
View Journal | View Issue

Cite this: RSC Adv., 2016, 6, 34600

Ni/H-ZSM-5 as a stable and promising catalyst for CO_x free H_2 production by CH_4 decomposition†

Chatla Anjaneyulu,[a] Gutta Naresh,[ac] Velisoju Vijay Kumar,[ac] Aytam Hari Padmasri,[b] James Tardio,[c] Suresh Kumar Bhargava[c] and Akula Venugopal*[a]

Received 11th February 2016
Accepted 30th March 2016

DOI: 10.1039/c6ra03857c

www.rsc.org/advances

Catalytic decomposition of methane for CO_x free hydrogen production is carried out over Ni supported on H-ZSM-5 catalysts with different Si/Al ratios (*i.e.* 40, 150, 300 and 485) at 550 °C and atmospheric pressure. Methane decomposition activity of Ni/H-ZSM-5 is decreased with time on stream and finally deactivated completely. The fresh and reduced catalysts are characterized by BET-SA, XRD, FT-IR, UV-DRS, TPR, pulse chemisorption of H_2 and N_2O and some of the used catalysts are characterised by CHNS, SEM, TEM and Raman spectroscopy. Raman spectra of the used catalysts showed both ordered and disordered carbon at 1580 cm^{-1} and 1320 cm^{-1}. The 20 wt% Ni/H-ZSM-5 (Si/Al = 150) exhibited a higher H_2 production rate over the other Ni loadings. The superior performance of 20 wt% Ni/H-ZSM-5 (Si/Al = 150) is rationalized by the physico-chemical properties of the various Ni loaded H-ZSM-5 catalysts.

1. Introduction

Hydrogen is a versatile and efficient fuel, which undergoes clean combustion as water is the only product generated.[1] Hence it is regarded as a promising energy vector in both transport and power generation sectors. Nowadays, most hydrogen is produced by steam reforming of methane, which is accompanied by large emissions of CO_2.[2] Thus, all the carbon contained in the raw methane ends up as CO_2, a greenhouse gas. There are several processes for the production of hydrogen and two of them are steam and auto thermal reforming of natural gas. Although these processes are mature technologies, they are somewhat complex and contain multisteps. In addition, CO free H_2 is highly desirable for use in PEM fuel cells as CO poisons the Pt electrode. The direct cracking of methane over supported nickel catalysts is an alternative route for the production of hydrogen from natural gas.[3,4] Methane decomposition reaction is a moderately endothermic process. The energy required per mole of hydrogen produced (45.0 kJ mol^{-1} H_2 at 600 °C) is less than that for the steam reforming of methane (48.0 kJ mol^{-1} H_2). Unlike the steam reforming process, the catalytic decomposition of methane (CDM) process does not include water gas shift and preferential oxidation of CO, which considerably simplifies the process and cost of hydrogen production.[5–7]

$$CH_4 \rightarrow C + 2H_2;\ \Delta H^\circ = 75.6\ \text{kJ mol}^{-1}$$

This hydrogen can be used as a clean energy for fuel-cells and the produced carbon can be used as functional material, such as fibres, graphite, carbon black, composites and catalyst supports. Here it is noteworthy to mention that carbon alone can be used as a catalyst for CDM but only at high temperatures (>750 °C).[8] Nickel is a common transition metal used for the conversion of methane.[9–16] The most important factors that influence the carbon deposits during methane decomposition are the particle size, dispersion and stabilization of the metallic nickel particle by selecting appropriate support. Michalkiewicz and co-workers critically reviewed the effect of reaction temperature on the carbon growth due to the Ni loading and also the nature of support that would strongly influence the H_2 yields as well as the quality of the CNTs formed during the CDM process.[17–19] Takenaka *et al.*[20] reported that a typical 40% Ni/SiO_2 catalyst with the nickel particle size of 60–100 nm that could give the carbon yield of as high as 491 g_C $(g_{Ni})^{-1}$ during methane decomposition at 550 °C. Furthermore, Ermakova *et al.*[21] reported the 90 wt% Ni/SiO_2 catalyst with the nickel particle of 10–40 nm size provided carbon yields in the order of 385 g_C $(g_{Ni})^{-1}$ at 550 °C. Other supports, such as TiO_2, MgO, ZrO_2 and Al_2O_3 gave relatively lower carbon yields.[22] Though the activated carbon and carbon blacks were explored for CDM, due to their lower activity, metal catalysts particularly Ni based

[a]Catalysis Laboratory, Inorganic & Physical Chemistry Division, CSIR-Indian Institute of Chemical Technology, Tarnaka – 500007, Hyderabad, Telangana, India. E-mail: akula@iict.res.in; Fax: +91-40-27160921; Tel: +91-40-27191720; +91-40-27193510

[b]Department of Chemistry, University College for Women Osmania University, Koti, Hyderabad – 500 095, Telangana, India

[c]Centre for Advanced Materials & Industrial Chemistry (CAMIC), School of Applied Sciences, RMIT University, GPO BOX-2476, Melbourne 3001, Australia

† Electronic supplementary information (ESI) available. See DOI: 10.1039/c6ra03857c

catalysts were found to be better than the other transitional metal catalysts.[23–26] A recent review emphasized the importance of modelling studies and regeneration of the catalysts in the catalytic decomposition of CH_4.[27] Choudhary *et al.* observed the formation of small amount of CO during CH_4 decomposition over Ni/H-ZSM-5 catalyst.[28] We believe that CO formation is occurring due to incomplete reduction of catalyst during the reductive pretreatment (Fig. S1†). Presence of ionic Ni species may be a reason for the formation of CO during the CDM process. In the present study Ni supported on H-ZSM-5 with varied Si/Al ratio samples were reduced at 550 °C for 2 h prior to the reaction; surprisingly formation of CO_x compounds was absent during the CDM reaction.

Hence the present work is undertaken to explore the catalytic performance of Ni supported on H-ZSM-5 with four different Si/Al ratios *i.e.* 40, 150, 300 and 485 for methane decomposition at reaction temperature of 550 °C. The activity and stability of catalysts is discussed based on the Ni metal surface area in conjunction with Raman spectra of deactivated samples.

2. Experimental

2.1 Catalysts preparation

The Ni/H-ZSM-5 samples were prepared by a simple incipient wet impregnation method. Here we have chosen H-ZSM-5 as a support with different Si/Al ratio (*i.e.* Si/Al ratio = 40, 150, 300 and 485 mole ratio). The zeolite support is commercially available; H-ZSM-5 Si/Al = 40, surface area = 600 $m^2\ g^{-1}$, Si/Al = 150 surface area = 470 $m^2\ g^{-1}$, Si/Al = 300 surface area = 340 $m^2\ g^{-1}$ and (Si/Al = 485; surface area = 450 $m^2\ g^{-1}$ prepared by us, see ESI†) supplied by M/s. Sud Chemie India Private Limited. In a typical impregnation method the required amount of nickel nitrate [$Ni(NO_3)_2 \cdot 6H_2O$] was taken to give required Ni loading with known amount of water in a 100 ml beaker and mixed with the requisite amount of support material to yield the respective Ni wt% needed. These solutions were dried with constant stirring at 100 °C until the sample gets dried and then kept for drying at 100 °C for about 24 h, followed by calcination in air at 550 °C for 5 h. Thus, prepared catalysts were used for evaluating CDM activities.

2.2 Catalysts characterisation

The XRD patterns of the samples were obtained on a Rigaku miniflex X-ray diffractometer using Ni filtered Cu K_α radiation (λ = 1.5406 Å) from 2θ = 10 to 80° at a scan rate of 2° min^{-1} with the beam voltage and a beam current of 30 kV and 15 mA respectively. The surface areas of the fresh catalysts were measured by N_2 physical adsorption at −196 °C in an Autosorb-I (Quantachrome) instrument. The specific surface area was calculated applying the BET method. The SEM images of the fresh and used catalysts were recorded using a JEOL-JSM 5600 instrument. For TEM analysis the samples dispersed in methanol solution and suspended on a 400 mesh, 3.5 mm diameter Cu grid and images were taken using JEOL JEM 2010 high-resolution transmission electron microscope. The Raman spectra for the structural characterization of deposited carbon in deactivated catalysts have been acquired with a Horiba Jobin-Yvon lab ram HR spectrometer using a laser beam excitation of λ = 632.81 nm. The infrared spectra were recorded between 4000 and 400 cm^{-1} at room temperature in a Agilent cary 600 FT-IR spectrometer. The carbon contents in deactivated catalysts are measured with VARIO EL analyser instrument. The UV-Vis spectra were recorded at room temperature using a UV-2000, Shimadzu spectrophotometer equipped with a diffuse reflectance attachment with an integrating sphere containing $BaSO_4$ as a reference. The spectra were recorded in the range between 190 and 800 nm with sampling interval 0.5 nm and slit width 2 nm and spectra were converted to Kubelka–Munk function.

The TPR analysis was carried out in a quartz micro-reactor interfaced to GC with TCD unit. About 50 mg of sample was loaded in an isothermal zone of a quartz reactor (i.d = 0.6 cm, length = 30 cm) heated by an electric furnace at a rate of 10 °C min^{-1} to 300 °C in flowing helium gas at a flow rate of 30 ml min^{-1}. After degassing the sample was cooled to room temperature then the helium gas switched to 5% H_2 in argon (30 ml min^{-1}) and the temperature was increased to 700 °C at a ramping rate of 5 °C min^{-1}. Hydrogen consumption measured by analyzing effluent gas by means of thermal conductivity detector and the H_2 uptakes were estimated with a calibration TPR of Ag_2O under similar protocol. Hydrogen chemisorption measurements were carried out on a Varian 3800 instrument. Prior to H_2 adsorption ~100 mg of the sample was reduced in a flow of hydrogen (30 ml min^{-1}) at 550 °C for 2 h and flushed out in a pure argon (Ar) gas flow (purity 99.995%) for an hour at 550 °C. The sample was subsequently cooled to 60 °C temperature in Ar gas stream. Hydrogen uptake was determined by injecting pulses of 5% hydrogen balance argon from a calibrated loop connected to on-line sampling valve in Ar stream passing the over the reduced sample. The nickel metal surface area was calculated assuming a stoichiometry of one hydrogen molecule per two surface nickel atoms using an atomic cross-sectional area of 6.49×10^{-20} m^2 per Ni atom. The H_2 adsorption was deemed to be complete after at least three successive peaks showed the similar GC areas.[29] N_2O pulse titration experiments were performed to analyze the Ni dispersion, size and Ni metal surface area[30,31] using Varian 3800 series system equipped with a thermal conductivity detector (TCD). The catalysts of 50–100 mg were placed in the quartz tube and reduced to 550 °C for 1 h in 5% H_2/Ar prior to the test. He gas was used as carrier gas at 30 ml min^{-1}, and the successive pulses of pure N_2O gas were subsequently introduced into He stream by means of a calibrated sampling valve at a temperature of 90 °C. The product gases (N_2 and N_2O) were analyzed by Porapak N column using GC with TCD.

2.3 Methane decomposition activity measurements

The catalytic activities were performed at 550 °C at atmospheric pressure in a fixed-bed vertical quartz reactor (i.d = 1 cm, length = 46 cm) operated in a down flow mode heated by an electric furnace. Methane supplied by Bhuruka gases limited (99.99%) was used directly without further purification. Many of the experimental conditions adopted were same as reported earlier[8]

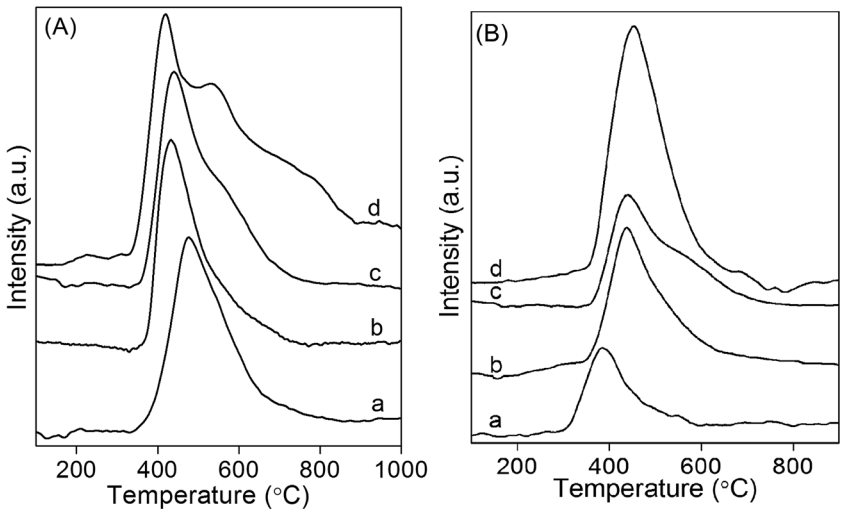

Fig. 1 (A) TPR profile of (a) 30 wt% Ni/H-ZSM-5 (Si/Al = 40), (b) 30 wt% Ni/H-ZSM-5 (Si/Al = 150) and (c) 30 wt% Ni/H-ZSM-5 (Si/Al = 300) and (d) 30 wt% Ni/H-ZSM-5 (Si/Al = 485) catalysts, (B) Ni loading on H-ZSM-5 (Si/Al = 150) catalysts (a) 10, (b) 20, (c) 30 and (d) 50 wt%.

and some of the details were: a catalyst charge of ~20 mg, with methane flow rate = 30 ml min^{-1}, *i.e.* GHSV of 90 l h^{-1} $(g_{cat})^{-1}$. Prior to the reaction, the catalyst was reduced at 550 °C with 5% H_2 in Ar for 2 h. The reaction was continued until all the catalysts were deactivated. Then, obtained catalysts were weighed and after each experiment. The outflow gas was analyzed online by gas chromatography equipped with a carbosphere column and TCD detector using N_2 as a carrier. The conversion of methane was determined using calibrated data. The first analysis was done 10 min after methane was passed over the catalyst.

3. Results

3.1 FT-IR analysis

The 30 wt% Ni supported on zeolite with different Si/Al mole ratios are analysed by FTIR spectroscopy (see ESI†). The absorption bands near 788, 1084 and 1218 cm^{-1} are characteristic of SiO_4 tetrahedron units.[32,33] The strong absorption band in the region 1000–1200 cm^{-1} has been assigned to the internal vibration of SiO_4, AlO_4 tetrahedra for ZSM-5.[34] The band around 1084 cm^{-1} is attributed to the internal asymmetric stretching vibration of Si–O–Si linkage and is found to be shifted towards higher wave number with increasing Si/Al ratio. The band near 788 cm^{-1} is assigned to the symmetric stretching of the external linkages and the strong band near 543 cm^{-1} is ascribed to the double five-ring lattice vibration of the external linkages[35] (Fig. S2A†). The vibrational band around 450 cm^{-1} is due to the T–O bending vibrations of the SiO_4 and AlO_4 internal tetrahedra. The absorption bands around 543 and 450 cm^{-1} are characteristic of the ZSM-5 crystalline structure.[36] The sample with various Ni loadings on H-ZSM-5 (Si/Al = 150) (Fig. S2B†) exhibited bands at 1230 cm^{-1}, 1100 cm^{-1} and 796 cm^{-1} that are attributed to the Si–O–Si asymmetric and symmetric stretching frequencies as well as internal stretching frequencies of H-ZSM-5. The band near 3429 cm^{-1} indicates that there are plenty of –OH groups on Ni/H-ZSM-5 surface. The band at 1625 cm^{-1} is attributed to adsorbed water, and these results are similar to the earlier reports.[37]

3.2 XRD analysis of fresh calcined and reduced catalysts

The powder XRD patterns of 30 wt% Ni loaded on H-ZSM-5 (with Si/Al = 40, 150, 300 and 485) fresh samples showed the reflections at $2\theta = 37.28°$, 43.3°, 62.9° and 75.3° pertaining to

Table 1 Physicochemical properties of Ni supported on H-ZSM-5 catalysts

Ni/H-ZSM-5	Si/Al ratio	BET-SA (m^2 g^{-1})	NiO crystallite size[a] (nm)	Ni domain size[b] (nm)	H_2 uptake[c] (μmol g_{cat}^{-1})
30 wt% Ni	40	220	29	25	2121
30 wt% Ni	150	396	21	29	2058
30 wt% Ni	300	255	25	27	2035
30 wt% Ni	485	326	27	31	2023
10 wt% Ni	150	432	12	22	525
20 wt% Ni	150	406	16	25	985
50 wt% Ni	150	265	23	32	2482

[a] From XRD patterns of calcined samples. [b] XRD patterns of reduced samples. [c] H_2 uptakes measured from TPR analysis with a calibrated Ag_2O TPR.

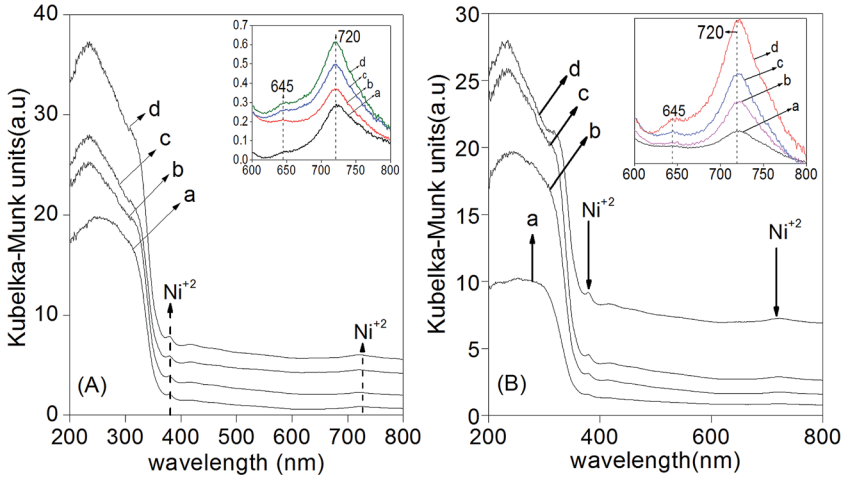

Fig. 2 (A) UV-Vis diffuse reflectance spectra of calcined 30 wt% Ni supported on H-ZSM-5 with (a) Si/Al = 40, (b) Si/Al = 150, (c) Si/Al = 300 and (d) Si/Al = 485 catalysts, (B) Ni loaded on H-ZSM-5 (Si/Al = 150) catalysts, (a) 10, (b) 20, (c) 30 and (d) 50 wt%.

crystalline NiO phase [ICDS# 01-1239], along with minor diffraction lines of H-ZSM-5 phase (Fig. S3A†). The (Ni loaded) fresh calcined 10–50 wt% Ni/H-ZSM-5 (Si/Al ratio = 150) samples also confirmed both NiO and H-ZSM-5 phases. Increase in Ni loading, intensity of NiO diffraction lines are increased due to formation of larger crystallites (Fig. S3A†). The XRD patterns of 30 wt% Ni/H-ZSM-5 samples (reduced) displayed the metallic Ni phase [ICDS# 87-0712] (Fig. S4A and B†).

3.3 H_2-TPR analysis

The TPR patterns of Ni loaded H-ZSM-5 samples presented in Fig. 1A, and the H_2 uptakes are reported in Table 1. The 30 wt% Ni/H-ZSM-5 exhibited the T_{max} 540 °C ascribed to reduction of bulk NiO species. The H_2 uptakes are more or less same, over the 30 wt% Ni/H-ZSM-5 (with varied Si/Al ratio), whereas a linear increase (Table 1) with increase in Ni loading is found. This suggests the bulk property of H_2-TPR. Fig. 1B, exhibit broad curves due to NiO in two stage reduction. The low temperature peak (380–450 °C) is assigned to dispersed and the high temperature (~575 °C) peak is mainly due to large sized NiO clusters.

It is also observed that at higher Ni loadings the reduction peak is sharpened [50 wt% Ni/H-ZSM-5 (Si/Al = 150)]. XRD analysis of these samples demonstrated the increase in NiO domain size (Table 1) at higher Ni loadings. Based on these results it is concluded that reduction peak at 450 °C and 575 °C are due to NiO species that are located at outer surface and sodalite cages of zeolite crystals respectively.[38]

3.4 UV-DRS analysis

As shown in Fig. 2A the UV-DR spectra were nearly the same, irrespective of the varied Si/Al mole ratio in zeolite. The absorption bands at 240, 310 nm are originating from O → Ni charge transition are stronger (Fig. 2B).[39] The bands at 715 nm and 377 nm represent the octahedrally coordinated Ni^{2+} species

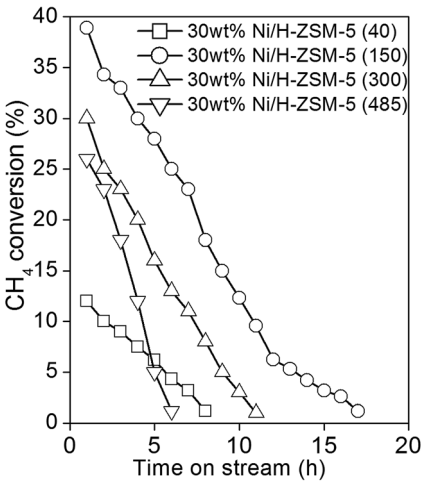

Fig. 3 Methane conversion (%) with time (h) over 30 wt% Ni/H-ZSM-5 (Si/Al = 40, 150, 300 and 485) catalysts at 550 °C temperature.

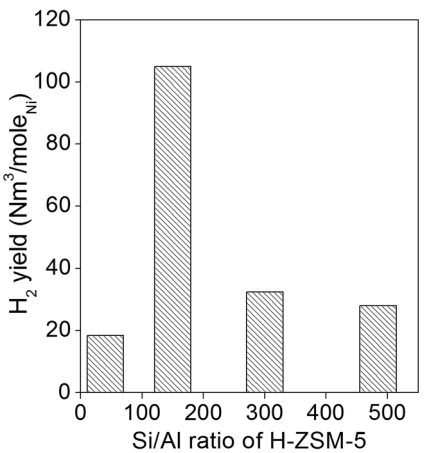

Fig. 4 Hydrogen yields during methane decomposition over 30 wt% Ni/H-ZSM-5 with varying Si/Al mole ratio.

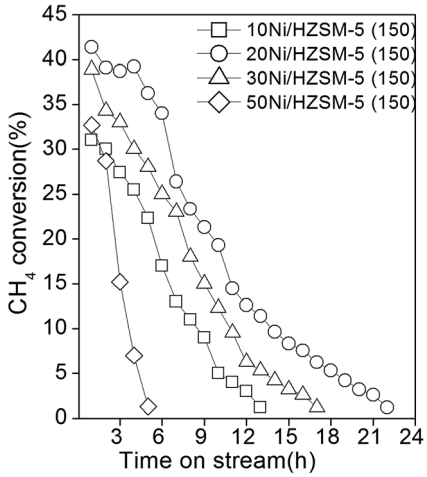

Fig. 5 Methane conversions (%) with time (min) over Ni loading on Ni/H-ZSM-5 (Si/Al ratio = 150) catalysts at 550 °C temperature.

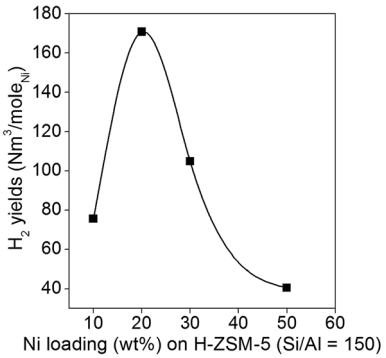

Fig. 6 Carbon yields during methane decomposition as a function of Ni loading over Ni/H-ZSM-5 (Si/Al ratio = 150) catalysts.

in NiO lattice, while the absorption signal in the range of 600–645 nm assigned to the tetrahedrally coordinated Ni^{2+} species.[40] It is clearly evident that the band intensity of 720 nm peak is increased upon increasing the Ni loading (Fig. 2B).

3.5 Influence of Si/Al ratio on CDM activity of Ni/H-ZSM-5

The influence of Si/Al ratio is examined keeping 30 wt% nickel (arbitrarily fixed) in the Ni/H-ZSM-5 catalysts, and the TOS analysis of these catalysts is reported in Fig. 3. It shows that all the catalysts were deactivated after certain time. In the comparative analysis 30 wt% Ni/H-ZSM-5 with Si/Al ratio = 150 displayed better activity and longevity of 17 h with a H_2 yield of 105.2 $Nm^3\ mol_{Ni}^{-1}$. The yields were estimated from the kinetic curves of the methane conversion to carbon and hydrogen proceeded stoichiometrically. The high H_2 yield (105.2 $Nm^3\ mol_{Ni}^{-1}$) on 30 wt% Ni/H-ZSM-5 (Si/Al ratio = 150) catalyst is substantiated the sustainability and longevity compared to 30 wt% Ni supported on Si/Al with 40, 300 and 485 H-ZSM-5 samples (Fig. 4). It should be mentioned here that none of these samples showed the formation of carbon oxides (CO and CO_2) unlike Choudhary *et al.* who found certain amount of CO during the CH_4 decomposition over Ni/H-ZSM-5 catalysts.[28] Hence various Ni loadings on H-ZSM-5 (with Si/Al = 150) samples are evaluated for CDM process.

3.6 Influence of Ni loading on CDM activity

Fig. 5 shows in methane conversion (%) as a function of time (h) during the catalytic decomposition of methane at 550 °C over Ni/H-ZSM (Si/Al = 150) catalysts with different Ni loadings from 10 to 50 wt%. The activity measurements were carried out under similar reaction conditions in order to optimize Ni loading on H-ZSM-5 (Si/Al = 150) zeolite. It is clear from Fig. 5 that methane conversion is found to be high in the initial stages and decreased rapidly or gradually with time on stream as a result of carbon deposition. The catalyst deactivation is attributed due to the deposition of carbon on the catalyst surface/active sites or accumulated at the entrance of the pores by pore blockage. The reaction run time until complete deactivation of the catalysts are in the order 50 < 10 < 30 < 20 wt% of Ni over H-ZSM-5 zeolite. Therefore the 20 wt% Ni is optimum for H-ZSM-5 (Si/Al = 150) that showed a better H_2 yield of 171 $Nm^3\ mol_{Ni}^{-1}$ and longevity compared to other catalysts.[12]

It was reported that CH_4 decomposition takes place on surface Ni sites followed by deposition of carbon by generating gaseous H_2. According to earlier reports, carbon deposition on Ni surface and diffusion of deposited carbon through Ni particle to the interface where it gets precipitated in the form of graphitic carbon as CNTs and/or CNFs occurs simultaneously. The carbon accumulation would be high when the rate of carbon deposition on the Ni surface is lower than the rate of carbon diffusion through Ni particle. If the reverse is true then the catalyst deactivates rapidly consequently lower H_2 yields are

Table 2 CDM activity data and Ni metal surface areas of Ni/H-ZSM-5 with varied Si/Al ratio

Ni/H-ZSM-5	Si/Al ratio	H_2 uptake[a] (μmol g_{cat}^{-1})	S_{Ni}[a] ($m^2\ g_{cat}^{-1}$)	N_2O uptake[b] (μmol g_{cat}^{-1})	S_{Ni}[b] ($m^2\ g_{cat}^{-1}$)	H_2 yield[c] ($Nm^3\ mol_{Ni}^{-1}$)
30 wt% Ni	40	45	3.4	39.8	1.6	18.4
30 wt% Ni	150	85	6.4	101.9	4.0	105.2
30 wt% Ni	300	63	4.7	56.0	2.2	31.8
30 wt% Ni	485	59	4.1	47.4	1.9	28.2
10 wt% Ni	150	75	5.6	83.4	3.3	75.6
20 wt% Ni	150	124	9.3	120.2	4.8	171.0
50 wt% Ni	150	70	5.2	94.9	3.7	40.6

[a] H_2 pulse chemisorption. [b] N_2O titration. [c] CDM activity.

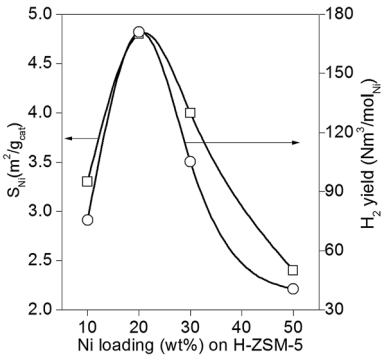

Fig. 7 Relationship between Ni metal surface area and H_2 yields *vs.* Ni loading on H-ZSM-5 (Si/Al = 150).

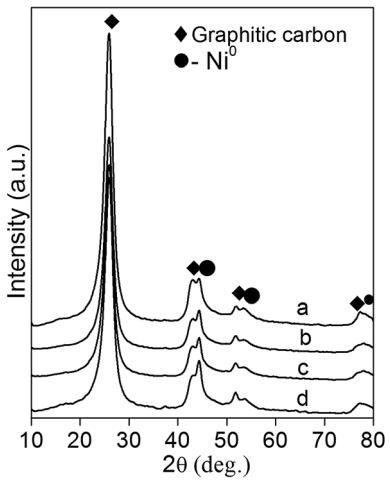

Fig. 8 XRD patterns of deactivated 30 wt% Ni/H-ZSM-5 with Si/Al ratio (a) 40, (b) 150, (c) 300 and (d) 485 catalysts.

observed.[41] The typical volcano shape relationship obtained (Fig. 6) with carbon formed per g_{Ni} (C/Ni) of the catalyst with increase Ni loading, indicates how critical is the role of metal loading on the catalyst performance during the CDM process. The H_2 yields are increased in the order of 50 < 10 < 30 < 20 wt% Ni/H-ZSM-5 (Si/Al = 150). A similar observation of volcano type tendency on H_2 yields over Ni/SiO_2 catalysts during the catalytic decomposition of methane is reported.[12]

4. Discussion

The Ni metal surface areas of Ni/H-ZSM-5 samples measured by H_2 pulse chemisorption and the results are reported in Table 2.[26] Fig. 7 demonstrated a linear relationship between the Ni metal surface area and the H_2 yields obtained from CDM results. Thus it is concluded that the H_2 production rate is dependent up on the Ni metal surface area of Ni/H-ZSM-5 (Si/Al ratio = 150) catalysts. It has also been observed that the H_2 rates are in good correlation with the Ni metal surface areas of the catalysts measured by N_2O decomposition studies (Table 2). High dispersion of Ni over 20 wt% Ni/H-ZSM-5 could be a possible for the higher H_2 yields than the other Ni loaded samples.

Fig. 8 reveals the XRD patterns of deactivated 30 wt% Ni/H-ZSM-5 (Si/Al = 40, 150, 300 and 485) catalysts recovered after CDM reaction. The irreversible carbon that is deposited on the catalyst appeared as graphitic carbon in XRD analysis. The strong reflections at 2θ = 26.1°, 42.9°, 53.8° and 77.7° are attributed to the graphitic carbon [ICSD# 01-0640] and weak diffraction lines due to metallic Ni at 2θ = 44.2°, 51.7° and 76.4°.

The nature of deposited carbon is confirmed by Raman spectra of the Ni/H-ZSM-5 catalysts and results are presented in Fig. 9A and B. The Raman spectra displayed two distinct bands centered at around 1320 cm^{-1} (D-band) attributed to structural imperfection of graphite or the presence of carbon nanoparticles and amorphous carbon. The band at 1580 cm^{-1} (G-band) ascribed to the in-plane carbon–carbon stretching vibrations rather ordered structure carbon.[18,42,43]

The degree of crystallinity of deposited carbon can be obtained from the frequency and intensity of Raman 'D' and 'G' bands. The ratio of peak area of the 'D' band to that of the 'G'

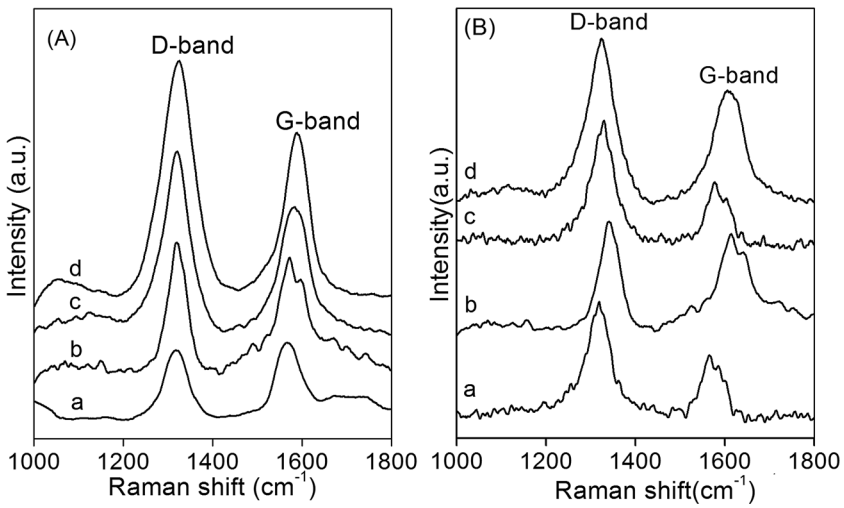

Fig. 9 Raman spectra of deactivated (A) different Si/Al ratio Ni/H-ZSM-5 (Si/Al: 40, 150, 300 and 485) and (B) Ni loadings of Ni/H-ZSM-5 (Si/Al ratio = 150) catalysts.

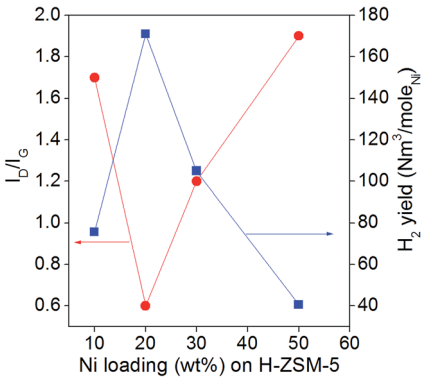

Fig. 10 The I_D/I_G ratio and H_2 yields against various Ni loaded H-ZSM-5 (Si/Al = 150) deactivated catalysts.

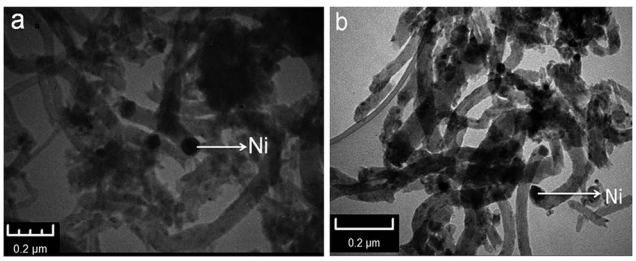

Fig. 11 TEM images of spent (a) 30 wt% Ni/H-ZSM-5 (Si/Al = 150); and (b) 20 wt% Ni/H-ZSM-5 (Si/Al = 150) catalysts.

band *i.e.* I_D/I_G is considered as an index for the crystalline order of graphite which is inversely proportional to the average plane size of the perfect graphenes; that is the graphitization degree of carbon is higher at lower I_D/I_G values (Fig. 10).[19,44]

The morphology of deposited carbon can be determined using SEM analysis. The SEM images of 30 wt% Ni/H-ZSM-5 with Si/Al = 40, 150 and 300 (Fig. S5†) showed agglomerated clusters (Fig. S5A†), spherical (Fig. S5B†) and large size clusters of Ni particles (Fig. S5C†). Formation of carbon nanotubes is evident in their respective deactivated samples. It appears that the deposited carbon is in nanosize and few micrometers in length of filamentous carbon. On the other hand, the size and length of deposited filaments varied with variation in Si/Al ratios. The nature of filamentous carbon is further evidenced from TEM image of deactivated Ni/H-ZSM-5 samples (Si/Al = 150) (Fig. 11). It is also found that the Ni metal is occupied at the tip of the carbon filament. The size of the produced filament is more or less similar to Ni particle size (~30 nm) occupied at the tip of the carbon nanofiber.[17,45,46] These results are in good agreement with the mechanisms proposed earlier for filamentous carbon growth, according to which the diameter of carbon nanofibers must be approximately equal to the size of Ni particle at the tip of the carbon nanofiber.[47]

5. Conclusions

The 30 wt% Ni loaded on H-ZSM-5 zeolite with varied Si/Al ratios were examined for the CO_x free hydrogen production. The optimized Si/Al = 150 (H-ZSM-5) has been further explored with different Ni loadings. The catalyst with 20 wt% Ni supported on H-ZSM-5 with Si/Al = 150 demonstrated tremendously higher H_2 yields than the other compositions under identical experimental condition. The SEM and TEM images revealed the presence of carbon nanofibers in all the deactivated samples. The normalized intensities of Raman spectra with I_D/I_G *vs.* Ni loadings defined the higher amount of ordered carbon over 20 wt% Ni/H-ZSM-5 (Si/Al = 150) thus produced higher H_2 yields (171 Nm^3 mol_{Ni}^{-1}). The superior performance of this catalyst can also be explained by the higher Ni metal surface area of 20 wt% Ni/H-ZSM-5 (Si/Al = 150) catalyst. A direct correlation between Ni loading *vs.* H_2 yields and Ni metal surface area is observed. Further studies are in progress on the differences in morphology of various Si/Al ratios of H-ZSM-5 for Ni in the CO_x free hydrogen production by catalytic decomposition of methane.

Acknowledgements

The authors CA thank CSIR New Delhi, VVK and GN thanks CSIR-IICT for providing necessary facilities.

References

1 T. V. Choudhary and D. W. Goodman, *Catal. Today*, 2002, **77**, 65.
2 Y. Matsumura and T. Nakamori, *Appl. Catal., A*, 2004, **258**, 107.
3 N. Z. Muradov, *Int. J. Hydrogen Energy*, 1993, **18**, 211.
4 N. Muradov, *Energy Fuels*, 1998, **12**, 41.
5 M. Steinberg and H. Cheng, *Int. J. Hydrogen Energy*, 1989, **14**, 797.
6 M. Steinberg, *Int. J. Hydrogen Energy*, 1998, **23**, 419.
7 M. G. Poirier and C. Sapundzhiev, *Int. J. Hydrogen Energy*, 1997, **22**, 429.
8 J. Ashok, S. Naveen Kumar, A. Venugopal, V. Durga Kumari and M. Subrahmanyam, *J. Power Sources*, 2007, **164**, 809.
9 A. C. Lua and H. Y. Wang, *Appl. Catal., B*, 2013, **132**, 469.
10 L. C. Chen and S. D. Lin, *Appl. Catal., B*, 2011, **106**, 639.
11 J. Li and K. J. Smith, *Appl. Catal., A*, 2008, **349**, 116.
12 A. Venugopal, S. Naveen Kumar, J. Ashok, D. Hari Prasad, V. Durga Kumari, K. B. S. Prasad and M. Subrahmanyam, *Int. J. Hydrogen Energy*, 2007, **32**, 1782.
13 H. Y. Wang and A. C. Lua, *J. Phys. Chem. C*, 2012, **116**, 26765.
14 I. Gonzalez, J. C. De Jesus, E. Canizales, B. Delgado and C. Urbina, *J. Phys. Chem. C*, 2012, **116**, 21577.
15 T. V. Reshetenko, L. B. Avdeeva, Z. R. Ismagilov, A. L. Chuvilin and V. A. Ushakov, *Appl. Catal., A*, 2003, **247**, 51.
16 M. A. Ermakova, D. Y. Ermakova, G. G. Kuvshinov and L. M. Plyasova, *J. Catal.*, 1999, **187**, 77.
17 B. Michalkiewicz and J. Majewska, *Int. J. Hydrogen Energy*, 2014, **39**, 4691.
18 J. Majewska and B. Michalkiewciz, *New Res. Carbon Mater.*, 2014, **29**, 102.

19 J. Ziebro, I. Lukasiewciz, E. Borowwiak-Palen and B. Michalkiewciz, *Nanotechnology*, 2010, **21**, 145308.
20 S. Takenaka, H. Ogihara and K. Otsuka, *J. Catal.*, 2002, **208**, 54.
21 M. A. Ermakova, D. Y. Ermakov and G. G. Kuvshinov, *Appl. Catal., A*, 2000, **201**, 61.
22 J. Li, G. Lu, K. Li and W. Wang, *J. Mol. Catal. A: Chem.*, 2004, **221**, 105.
23 H. F. Abbas and W. M. A. W. Daud, *Fuel Process. Technol.*, 2009, **90**(9), 1167.
24 H. F. Abbas and W. M. A. W. Daud, *Int. J. Hydrogen Energy*, 2009, **34**(15), 6231.
25 H. F. Abbas and W. M. A. W. Daud, *Int. J. Hydrogen Energy*, 2009, **34**(19), 8034.
26 J. Ashok, S. Naveen Kumar, A. Venugopal, V. Durga Kumari, S. Tripathi and M. Subrahmanyam, *Catal. Commun.*, 2007, **9**, 164.
27 H. F. Abbas and W. M. A. W. Daud, *Int. J. Hydrogen Energy*, 2010, **35**, 1160.
28 T. V. Choudhary, C. Sivadinarayana, C. C. Chusuei, A. Klinghoffer and D. W. Goodman, *J. Catal.*, 2001, **199**, 9.
29 K. V. R. Chary, P. V. Ramana Rao and V. Venkat Rao, *Catal. Commun.*, 2008, **9**, 886.
30 S. Tada, M. Yokoyama, R. Kikuchi, T. Haneda and H. Kameyama, *J. Phys. Chem. C*, 2013, **117**, 14652.
31 X. Y. Gao, J. Ashok, S. Widjaja, K. Hidajat and S. Kawi, *Appl. Catal., A*, 2015, **503**, 34.
32 L. Shirazi, E. Jamshidi and M. R. Ghasemi, *Cryst. Res. Technol.*, 2008, **43**, 1300.
33 L. Jiangyin, Z. Zhao, C. Xu, A. Duan and P. Zhang, *Catal. Lett.*, 2006, **109**, 65.
34 V. P. Shiralkar and A. Clearfield, *Zeolites*, 1989, **9**, 363.
35 W. Fan, R. Li, J. Ma, B. Fan and J. Cao, *Microporous Mater.*, 1995, **4**, 301.
36 P. A. Jacobs, H. K. Beyer and J. Valyon, *Zeolites*, 1981, **1**, 161.
37 G. Coudurier, C. Naccache and J. C. Vedrine, *J. Chem. Soc., Chem. Commun.*, 1982, 1413.
38 N. W. Hurst, S. J. Gentry, A. Jones and B. D. McNicol, *Catal. Rev.: Sci. Eng.*, 1982, **24**, 233.
39 D. Srinivas, C. V. V. Satyanarayana, H. S. Potdar and P. Ratnasamy, *Appl. Catal., A*, 2003, **246**, 323.
40 B. Vos, E. Poels and A. Bliek, *J. Catal.*, 2001, **77**, 198.
41 R. T. K. Baker, M. A. Barber, P. S. Harris, F. S. Feates and R. J. Waite, *J. Catal.*, 1972, **26**, 51.
42 C. Anjaneyulu, G. Naresh, V. Vijay Kumar, J. Tardio, T. Venkateshwar Rao and A. Venugopal, *ACS Sustainable Chem. Eng.*, 2015, **3**, 1298.
43 C. Anjaneyulu, S. Naveen Kumar, V. Vijay Kumar, G. Naresh, S. K. Bhargava, K. V. R. Chary and A. Venugopal, *Int. J. Hydrogen Energy*, 2015, **40**, 3633.
44 J. Ashok, P. Shiva Reddy, G. Raju, M. Subrahmanyam and A. Venugopal, *Energy Fuels*, 2009, **23**, 5.
45 J. Ashok, G. Raju, P. Shiva Reddy, M. Subrahmanyam and A. Venugopal, *Int. J. Hydrogen Energy*, 2008, **33**, 4809.
46 C. Anjaneyulu, V. Vijay Kumar, S. K. Bhargava and A. Venugopal, *J. Energy Chem.*, 2013, **22**, 853.
47 V. B. Fenelonov, A. Y. Derevyankin, L. G. Okkel, L. B. Avdeeva, V. I. Zaikovskii and E. M. Moroz, *Carbon*, 1997, **35**, 1129.